J. Fluid Mech. (1988), *vol.* 188, *pp.* 133–146
Printed in Great Britain

Breakup of fluid droplets in electric and magnetic fields

By J. D. SHERWOOD
Schlumberger Cambridge Research, P.O. Box 153, Cambridge CB3 0HG, UK

(Received 10 January 1986 and in revised form 14 August 1987)

A drop of fluid, initially held spherical by surface tension, will deform when an electric or magnetic field is applied. The deformation will depend on the electric/magnetic properties (permittivity/permeability and conductivity) of the drop and of the surrounding fluid. The full time-dependent low-Reynolds-number problem for the drop deformation is studied by means of a numerical boundary-integral technique. Fluids with arbitrary electrical properties are considered, but the viscosities of the drop and of the surrounding fluid are assumed to be equal.

Two modes of breakup have been observed experimentally: (i) tip-streaming from drops with pointed ends, and (ii) division of the drop into two blobs connected by a thin thread. Pointed ends are predicted by the numerical scheme when the *permittivity* of the drop is high compared with that of the surrounding fluid. Division into blobs is predicted when the *conductivity* of the drop is higher than that of the surrounding fluid. Some experiments have been reported in which the drop deformation exhibits hysteresis. This behaviour has not in general been reproduced in the numerical simulations, suggesting that the viscosity ratio of the two fluids can play an important role.

1. Introduction

The deformation of fluid interfaces under an applied field is a classical problem, and has been studied by many authors. Applications include the breakup of rain drops in thunderstorms, electrohydrodynamic atomization, the behaviour of jets and drops in ink-jets plotters, and the breakdown of insulating liquids via the deformation of impurities (e.g. water droplets) too small to be eliminated. A thorough review of electrohydrodynamics is given by Melcher (1963, 1981).

In this paper we shall study the deformation and breakup of a drop of fluid. At least two modes of breakup are observed experimentally. Conical points may be formed in the surface of the drop (Wilson & Taylor 1925; Mackay 1931; Allan & Mason 1962; Garton & Krasucki 1984; Taylor 1964). A fluid jet, or a series of droplets, or a fine mist, is then ejected from the tip of the cone. This conical instability is observed in other geometries, e.g. the instability of a horizontal plane surface (Taylor & McEwan, 1965), or electrohydrodynamic atomization from a capillary (reviewed by Kozhenkov & Fuks 1976). It is therefore not surprising that the numerical simulations to be presented in §3 will sometimes produce conical interfaces. However, we have not been able to follow the subsequent ejection of droplets from the tip of the cone.

Drop breakup can also occur via other mechanisms. Torza, Cox & Mason (1971) show photographs of drops which divide into two blobs connected by a thin thread. We shall later show that such behaviour can be expected when the fluids have non-

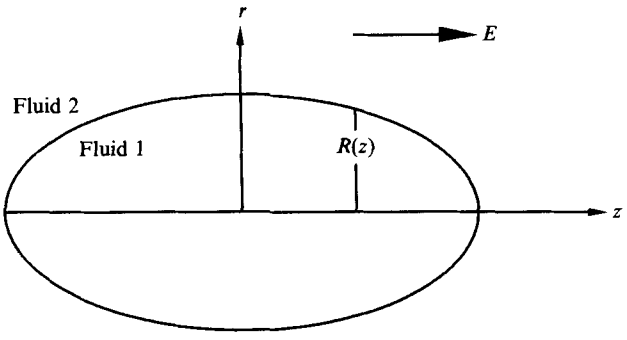

FIGURE 1. The drop of fluid 1 surrounded by fluid 2.

zero conductivities. Under these circumstances charge will build up at the fluid interface, on which tangential stresses will act. A drop will therefore deform, but even when equilibrium has been reached the fluid outside and within the drop will circulate because of the electric stresses (Taylor 1966). This topic is reviewed by Melcher & Taylor (1969).

The equivalent magnetic experiments can be performed in ferrofluids. Thus drop deformation has been studied by Arkhipenko, Barkov & Bashtovoi (1978), and by Drozdova, Skrobotova & Chekanov (1979), while sharp conical spikes can also occur, e.g. when a magnetic field is applied normal to a plane interface (Cowley & Rosensweig 1967). We shall consider, in particular, the experiments of Bacri, Salin & Massart (1982), and of Bacri & Salin (1982, 1983), on ferrofluid drop deformation. When the magnetic field was increased and subsequently reduced, hysteresis in the deformation of the drop was observed. We shall discuss these results when reviewing energy arguments which have been used to predict the drop shape. However, we must first introduce the notation that we require, and thus we now state the problem that we address in the rest of this paper.

1.1. *The problem to be studied*

We shall study the deformation of a drop of fluid 1 surrounded by fluid 2, under the influence of an electric field E (or magnetic field B) applied parallel to the z-axis (figure 1). We assume that the densities ρ_i $(i = 1,2)$ of the two fluids are identical, and equal to ρ^*; henceforth we neglect gravity. We shall also assume that the fluid viscosities are equal: $\mu_i^* = \mu^*$ $(i = 1,2)$, since the effect of the viscosity ratio merits a study in itself. In the absence of an applied field, interfacial tension (coefficient γ) will hold the drop spherical with radius a. If the electrical properties of the two fluids are not identical, then when an electric field is applied there will be a jump in the electric stress at the interface. The drop will therefore deform. When the fluids are perfect insulators, the drop deformation will depend on the ratio $\epsilon_0 E^2 a/\gamma$ of the electric stress to interfacial tension (ϵ_0 is the permittivity of free space, $\epsilon_0\epsilon_i$ the permittivity of fluid i), and on the ratio of the dielectric constants $\kappa = \epsilon_1/\epsilon_2$ of the two fluids. If the fluids are conductors, their conductivities σ_i will also be important. In the magnetic problem the permeabilities μ_i of the two fluids play a role entirely analogous to that of the permittivities, and there is no equivalent to the conductivities. We shall therefore fix our attention upon the more general electric problem. Nevertheless, it should be remembered that the magnetic problem has experimental advantages. If the drop acquires a net charge, electrophoresis will occur in an electric field, but not in a magnetic field.

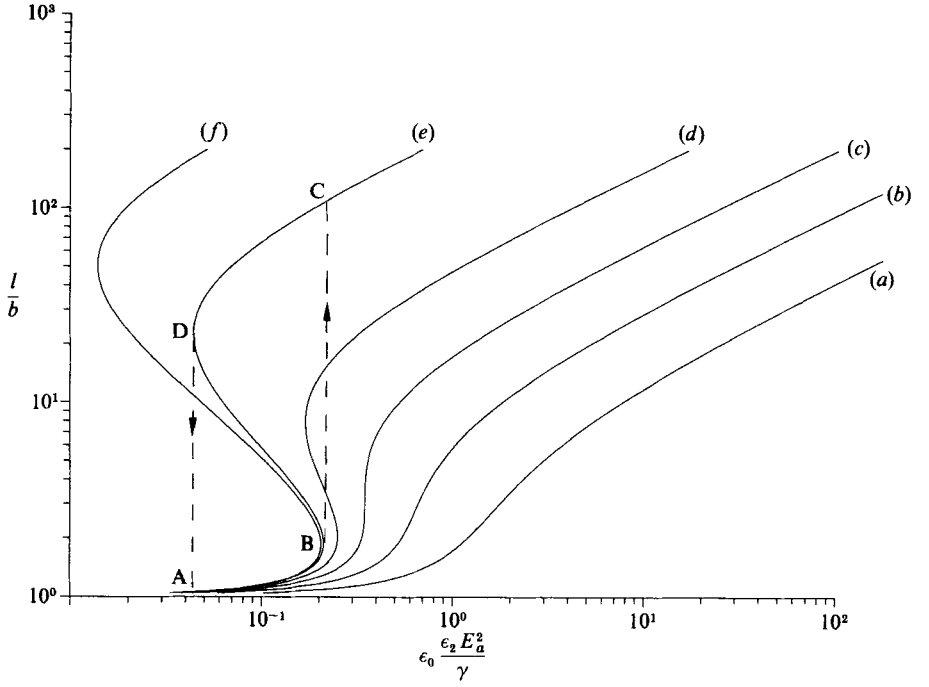

FIGURE 2. The aspect ratio l/b as a function of the field strength $\epsilon_0 \epsilon_2 E^2 a \gamma^{-1}$, as given by minimizing the energy of a spheroid. Permittivity ratios ϵ_1/ϵ_2 = (*a*) 5.0; (*b*) 10.0; (*c*) 20.8; (*d*) 50; (*e*) 250; (*f*) 1000.

1.2. *Minimum-energy arguments for the drop shape*

Techniques for making ferrofluids are sufficiently developed that fluids can be designed to separate into two phases. Drops of the concentrated phase, with high permeability, are immersed in the phase with lower permeability. When no magnetic field is applied, the drops are spherical, indicating an effective interfacial tension. Bacri & Salin (1982, 1983) performed experiments which they analysed by means of energy arguments (O'Konski & Thacher 1953; Garton & Krasucki 1964). We shall need their results, so we briefly repeat the analysis, using electrical notation and SI units.

To obtain analytic results, we assume that the drop takes the form of a prolate spheroid with major and minor axes $2l$, $2b$, aligned with the electric field. This approximation has been shown to be good (Garton & Krasucki) as long as the drop is not too long, when pointed ends occur; the results to be presented later support this view. The energy of a dielectric body with volume V introduced into an electric field $\boldsymbol{E}$ is

$$E_e = \tfrac{1}{2}\epsilon_0 \int_V (\epsilon_2 - \epsilon_1)\, \boldsymbol{E}\cdot\boldsymbol{E}_1 \, dv$$

where $\boldsymbol{E}_1$ is the field within V (Stratton 1958, p. 112). The field inside a dielectric spheroid can be obtained analytically, and hence the electrical energy E_e of the spheroid is

$$E_e = \tfrac{2}{3}\pi l b^2 \frac{\epsilon_0 E^2(\epsilon_1 - \epsilon_2)}{1 + \tfrac{1}{2}lb^2(1-\kappa^{-1})A_1},$$

where l/b is the aspect ratio of the drop, $e = (1-b^2/l^2)^{\frac{1}{2}}$ is the eccentricity, and

$$A_1 = -\left(2e - \ln\frac{1+e}{1-e}\right)(le)^{-3}.$$

The surface energy of the drop is simply

$$E_s = 2\pi\gamma(b^2 + lbe^{-1}\sin^{-1}e).$$

The drop is then assumed to take the form that minimizes the total energy $E_s + E_e$. Differentiating the above expressions, while holding the volume of the drop constant, we obtain the aspect ratio l/b as a function of the non-dimensionalized applied field $\epsilon_0 E^2 a/\gamma$, and the resulting deformation curves are shown in figure 2 for a series of permittivity ratios ϵ_1/ϵ_2. When $\epsilon_1/\epsilon_2 < 20.8$ the aspect ratio is single-valued. For higher values of ϵ_1/ϵ_2 hysteresis is possible, and this was observed by Bacri & Salin. They increased the field strength up to point B (figure 2). A slight increase in the field strength sufficed to substantially increase the drop length (point C). The downwards jump DA could also be observed.

When the aspect ratio $l/b \gg 1$, we may perform a slender-body analysis which removes the assumption that the drop is spheroidal. However, such an analysis sheds no light on the interesting region of field strengths and permittivity ratios in which breakup and hysteresis occur. A full numerical scheme was therefore adopted, and is discussed in the rest of this paper.

2. The time-dependent deformation of an arbitrary axisymmetric drop

We study the deformation of an arbitrary axisymmetric drop in an electric field. The problem falls naturally into two parts: that of finding the electric field, and that of determining the fluid motion. We resolve both Laplace's equation for the electric field, and Stokes' equations for the fluid motion, by means of the boundary-integral techniques. The electric problem has been studied by these methods by Miksis (1981) and by Brazier-Smith (1971). The hydrodynamic problem of flow around a rigid particle has been considered by Youngren & Acrivos (1975). Rallison & Acrivos (1978) and Rallison (1981) applied the technique to study drop deformation and breakup in extensional and general linear flows. B. Duffy & E. J. Hinch (unpublished) improved the numerical scheme and studied drop deformation in the presence of rigid walls. We shall in general adopt the refinements introduced by Duffy & Hinch.

At each time step a solution of Laplace's equation is obtained in terms of a distribution of singularities over the surface of the drop. The jump in the electric stress at the interface is computed, and this stress, together with interfacial tension, causes motion of the fluid. The surface of the drop is represented by a series of points which move with the fluid. Their position at the end of a time step Δt is computed, and we then re-solve Laplace's equation ready for the next time step. Eventually either (i) equilibrium is reached, or (ii) the drop length increases without bound, or (iii) the drop ends become sharp and pointed, followed by breakdown of the numerical scheme. If equilibrium is achieved, the applied electric field is increased and the process repeated. The choice of small increases in field strength ensures that the drop shape is never far from equilibrium.

The drop is assumed to be axially symmetric, with rounded ends (i.e. the radius of curvature of the tip is non-zero). We use cylindrical coordinates (r, z), and the drop

shape $r = R(z)$ is assumed to be a single-valued function of z. The surface of the drop is represented by $2N+1$ points (R_i, z_i), with $z_{2N+1} = -z_1 = l$, where l is the half-length of the drop. We assume symmetry about the midpoint $z_{N+1} = 0$. Associated with each point is the local surface density of singularities ρ_i. When interpolation is required, we assume that ρ_i, R_i, z_i can be expressed as quartic polynomials fitted through values at i, $i\pm1$, $i\pm2$. These interpolations are also used to determine $\boldsymbol{n}$ the normal to the surface, and the surface curvature.

2.1. *The electric field*

We consider the electric field to consist of two parts: the imposed field, and that due to the surface distribution of singularities ρ. The resulting field is computed as though in free space, and ρ, which we shall regard as a distribution of charge, is then picked such that the electric field E^{n} normal to the surface satisfies $\epsilon_1 E_1^{\mathrm{n}} = \epsilon_2 E_2^{\mathrm{n}}$ (or, when the fluids are conductors, we demand that $\sigma_i E_i^{\mathrm{n}}$ be continuous).

The potential ϕ at (r_x, x) due to a ring of unit charge density with radius r_y at y is

$$\phi(r_x, x) = \frac{1}{4\pi\epsilon_0}\int_0^{2\pi} [(x-y)^2 + r_x^2 + r_y^2 - 2r_x r_y \cos\theta]^{-\frac{1}{2}}\,\mathrm{d}\theta.$$

Integration of the charge density over the length of the drop yields the potential around the drop, and hence the electric field normal to the surface

$$E^{\mathrm{n}}(x) = \int_{-l}^{l} \frac{\rho(u)}{\pi\epsilon_0} R_y \left(\frac{1+R_y'^2}{1+R_x'^2}\right)^{\frac{1}{2}} \left(\frac{m}{4R_x R_y}\right)^{\frac{1}{2}} \left\{\frac{F(m)}{2R_x} + \frac{E(m)}{r_{xy}^2}\left(\frac{R_x^2 - R_y^2 - (x-y)^2}{2R_x} - R_x'(x-y)\right)\right\} \mathrm{d}y,$$

where

$$r_{xy}^2 = (x-y)^2 + (R_x - R_y)^2$$

and

$$m = \frac{4R_x R_y}{(x-y)^2 + (R_x + R_y)^2}.$$

$F(m)$ and $E(m)$ are complete elliptic integrals of the first and second kind respectively, and can be rapidly evaluated from polynomial approximation (Abramowitz & Stegun 1972). Note that in the above integral for E^n, r_{xy} goes through zero as y passes through x. All the singularities are integrable: they are subtracted out and handled analytically. The net result is the average field $\frac{1}{2}(E_1^n + E_2^n)$ due to charges on the surface. Brazier-Smith (1971) uses almost the same methods. He keeps the charge slightly within fluid 1, and consequently obtains E_2^n. Following Duffy & Hinch the integrals are performed by an averaged Simpson rule, the results of which we denote by $\Sigma g_{ij}\rho_j$ for appropriate coefficients g_{ij}. To this result we add the imposed uniform field E, and the total field normal to the interface at (R_i, z_i) is, in the case of dielectric fluids,

$$\Sigma\, g_{ij}\rho_j + \frac{\epsilon_0 E R_i'}{(1+R_i'^2)^{\frac{1}{2}}} = \frac{\rho_i(\kappa+1)}{2(\kappa-1)},$$

where the right-hand side has been determined by the requirement that ϵE^{n} be continuous across the interface. (When the conductivities are non-zero, we require σE^{n} continuous, and we merely replace $\kappa = \epsilon_1/\epsilon_2$ by σ_1/σ_2 in the above expression.) This set of equations is solved either by Gauss iteration, or by the IMSL routine LEQT2F (Gaussian elimination with equilibration, partial pivoting and iterative

improvement). Results obtained by the two methods are essentially identical, except just before breakup, when Gauss iteration might fail to converge. Computation times are similar, and the IMSL routine was generally used.

Knowing the charge density ρ, we can determine the tangential electric field

$$E^{\mathrm{t}}(r,z) = \int_{-1}^{l} \frac{\rho(y)}{\pi\epsilon_0} R_y \left(\frac{1+R_y'^2}{1+R_x'^2}\right)^{\frac{1}{2}} \left(\frac{m}{4R_xR_y}\right)^{\frac{1}{2}} \left\{R_x' \frac{F(m)}{2R_x} + \frac{E(m)}{r_{xy}^2}\left(\frac{(R_x^2-R_y^2-(x-y)^2)R_x'}{2R_x} + (x-y)\right)\right\} \mathrm{d}y.$$

2.2. *The stress tensor*

The discontinuity in electric field and in the permittivity across the interface causes a jump in the Maxwell stress tensor

$$\tau^{\mathrm{e}} = \epsilon_0\epsilon_i(E_iE_j - \tfrac{1}{2}\delta_{ij}|E|^2).$$

The jump in stress normal to the surface is

$$\tfrac{1}{2}\epsilon_0(\epsilon_2(E_2^{\mathrm{n}})^2 - \epsilon_1(E_1^{\mathrm{n}})^2 + (\epsilon_1-\epsilon_2)(E^{\mathrm{t}})^2),$$

which, for a perfect dielectric, becomes

$$\tfrac{1}{2}\epsilon_0\epsilon_2(1-\kappa^{-1})((E_2^{\mathrm{n}})^2 + \kappa(E_2^{\mathrm{t}})^2).$$

The jump in tangential stress is

$$\tfrac{1}{2}\epsilon_0 E^{\mathrm{t}}(\epsilon_2 E_2^{\mathrm{n}} - \epsilon_1 E_1^{\mathrm{n}}),$$

which is zero in the case of a perfect dielectric, and

$$\tfrac{1}{2}\epsilon_0\epsilon_2 E^{\mathrm{t}}\left(1-\kappa\frac{\sigma_2}{\sigma_1}\right)E_2^{\mathrm{n}}$$

when the conductivities are non-zero.

Note that the Maxwell stress tensor depends on the square of the electric field. Reversal of the field will leave our results unchanged. Experimentally, it is found that the sign of the applied potential can be important when a very fine mist is generated by electrohydrodynamic atomization (Vonnegut & Neubauer 1952).

To the normal electric stress we must add the jump in stress due to interfacial tension

$$\gamma\left(\frac{1}{R_1}+\frac{1}{R_2}\right) = \frac{\gamma}{R}\frac{(1+R'^2-RR'')}{(1+R'^2)^{\frac{3}{2}}},$$

where R_1 and R_2 are the principal radii of curvature of the surface.

These jumps in stress will cause motion of the fluid, which we examine in the following section.

2.3. *The fluid velocities*

We assume that the Reynolds number is sufficiently small for nonlinear inertial terms to be negligible, and it should be borne in mind that this assumption may be of dubious validity when a jet of fluid is ejected from a sharply pointed drop. We also neglect the inertial term $\rho^*\partial\boldsymbol{u}/\partial t$. This last assumption requires that the viscous

diffusion time $\rho^* a^2/\mu^*$ be small compared with the time $\mu^* a/\gamma$ required for relaxation of the drop shape to equilibrium, i.e. that

$$\frac{\rho^* \alpha \gamma}{\mu^{*2}} \ll 1.$$

(For studies of the opposite limit, in which $\mu^* \nabla^2 \boldsymbol{u} \ll \rho^* \mathrm{D}\boldsymbol{u}/\mathrm{D}t$, the reader is referred to Brazier-Smith, Jennings & Latham 1971.)

Under the above conditions, the stresses acting on the fluid are at all times in equilibrium, and we may use the representation of a general steady Stokes flow in terms of single and double layers of fundamental singularities, as discussed by Ladyzhenskaya (1969). It is useful to summarize the results, and we follow the presentation due to Rallison & Acrivos (1978). Let S be the surface of the drop, and

$$K_{ijk}(r) = \frac{-3}{4\pi} \frac{r_i r_j r_k}{r^5}, \quad J_{ij}(r) = \frac{\delta_{ij}}{r} + \frac{r_i r_j}{r}.$$

From the surface-integral representation of the Stokes flow exterior to S (fluid 2) we obtain a relation between the velocity $u_i(x)$ and stress $\sigma^2_{jk}(x)$ for $x, y \in S$:

$$\tfrac{1}{2} u_i(\boldsymbol{x}) + \int_{S_y} K_{ijk}(\boldsymbol{x}-\boldsymbol{y})\, u_j(\boldsymbol{y})\, n_k(\boldsymbol{y})\, \mathrm{d}S_y = -\frac{1}{8\pi\mu_2^*} \int_{S_y} J_{ij}(\boldsymbol{x}-\boldsymbol{y})\, \sigma^2_{jk}(\boldsymbol{y})\, n_k(\boldsymbol{y})\, \mathrm{d}S_y,$$

where $\boldsymbol{n}$ is the outward normal to the drop. Similarly, from an analysis of the flow within the drop,

$$\tfrac{1}{2} u_i(\boldsymbol{x}) - \int_{S_y} K_{ijk}(\boldsymbol{x}-\boldsymbol{y})\, u_j(\boldsymbol{y})\, n_k(\boldsymbol{y})\, \mathrm{d}S_y = -\frac{1}{8\pi\mu_1^*} \int_{S_y} J_{ij}(\boldsymbol{x}-\boldsymbol{y})\, \sigma^1_{jk}(\boldsymbol{y})\, n_k(\boldsymbol{y})\, \mathrm{d}S_y.$$

Hence

$$\tfrac{1}{2}(\mu_1^* + \mu_2^*)\, u_i(\boldsymbol{x}) + (\mu_1^* - \mu_2^*) \int_{S_y} K_{ijk}(\boldsymbol{x}-\boldsymbol{y})\, u_j(\boldsymbol{y})\, n_k(\boldsymbol{y})\, \mathrm{d}S_y$$
$$= -\frac{1}{8\pi} \int_{S_y} J_{ij}(\boldsymbol{x}-\boldsymbol{y})\, (\sigma^2_{jk} - \sigma^1_{jk})\, (\boldsymbol{y})\, n_k(\boldsymbol{y})\, \mathrm{d}S_y.$$

The right-hand side of this expression is merely the jump in stress across the interface, which is known. When $\mu_1^* = \mu_2^*$ the term in K_{ijk} vanishes. As explained by Rallison & Acrivos (1978) the flow is in this case generated by a membrane of forces f_i acting in an infinite homogeneous fluid. We shall restrict ourselves here to this simpler case, as we already have to investigate ranges of both the permittivity ratio ϵ_1/ϵ_2 and the conductivity ratio σ_1/σ_2. This restriction has the added advantage that while we must solve an integral equation for the charge density, the fluid velocities can be obtained by direct integration over the surface. Rallison & Acrivos considered arbitrary viscosity ratios, so there should in principle be no difficulty in extending the analysis to the more general case.

Since the problem is axisymmetric, the angular integrations can be performed analytically to yield

$$u(x) = (8\pi\mu^*)^{-1} \int_{-l}^{l} G_{ij}(x, y) f_j(y)\, R_y (1 + R'^2_y)^{\frac{1}{2}} \mathrm{d}y,$$

where the coefficients G_{ij} are given by Youngren & Acrivos:

$$G_{rr} = m^{-\frac{1}{2}} R_x^{-\frac{3}{2}} R_y^{-\frac{3}{2}} \{[R_x^2 + R_y^2 + 2(x-y)^2]F(m) - [2(x-y)^4 + 3(x-y)^2 (R_x^2 + R_y^2) + (R_x^2 - R_y^2)^2] r_{xy}^{-2} E(m)\}$$

$$G_{rz} = m^{-\frac{1}{2}}(x-y) R_x^{-\frac{3}{2}} R_y^{-\frac{1}{2}} \{F(m) + [R_x^2 - R_y^2 - (x-y)^2] r_{xy}^{-2} E(m)\}$$

$$G_{zr} = -m^{-\frac{1}{2}}(x-y) R_x^{-\frac{1}{2}} R_y^{-\frac{3}{2}} \{F(m) - [R_x^2 - R_y^2 + (x-y)^2] r_{xy}^{-2} E(m)\}$$

$$G_{zz} = 2m^{-\frac{1}{2}} R_x^{-\frac{1}{2}} R_y^{-\frac{1}{2}} \{F(m) + (x-y)^2 r_{xy}^{-2} E(m)\}.$$

G_{rr} and G_{zz} are singular at $y = x$. The singularities are subtracted and integrated analytically. The end points must clearly be treated as special cases. Unlike Duffy & Hinch, no advantages were found in according special treatment (with Gaussian integration) to the penultimate points (though the numerical problems here were such that an improved treatment would have been welcome).

Once the velocity has been computed, the position of the interface is advanced by a second-order Runge–Kutta scheme. Time steps are selected automatically on the basis of results for the first half of the time step. Δt is kept sufficiently small to maintain $R_i > 0$ $(i \neq 1, 2N+1)$ and $z_i - z_{i-1} > 0$. The chosen Δt might prove too long for the second half of the time step and pointed drops sometimes broke when R_2 or R_3 becomes negative. An isolated drop then appeared at the tip of the point: this apparent tip-streaming cannot be considered to be other than a numerical artefact.

As in all numerical schemes, errors are present. If the defining points are displaced perpendicular to the interface, the errors are controlled by surface tension. However, there is no physical mechanism to restore drift along the interface. When the conductivities are non-zero, the fluid is still in motion even when the equilibrium drop shape has been attained, and the defining points move towards the ends of the drop. If the fluids are perfect dielectrics, the numerical errors will ensure that the computed velocities are non-zero, and there is a tendency for the points to collect at the ends. At each time step the points are therefore repositioned along the interpolated interface in such a manner that the distance of separation is proportional to the local radius of curvature (within limits which prevent an absence of points at the drop centre). The points are therefore densest at the ends of the drop, where greater resolution is desirable. The use of higher powers of the radius of curvature, in order to increase still further the resolution at the tips, was found less satisfactory. Presumably the increased accuracy at the tips was gained at the expense of accuracy elsewhere.

With a numerical scheme we can never demand that the velocities be exactly zero at equilibrium. In general the requirement was that $|u_z| < u_{\max}$ (generally 10^{-2}) over the entire length of the drop. Merely requiring that $|u(z_1)|$ be small does not alone suffice, since the drop can oscillate about equilibrium. Nevertheless, this weaker requirement was adopted when conductivities were non-zero, since fluid velocities are not in general zero at equilibrium. Higher values of $u_{\max}$ were required at higher field strengths and aspect ratios. However, these had to be adopted with caution. If the drop was not in equilibrium when the applied electric field was increased, it was very easy to cause the drop to break, usually by the creation of pointed ends. It is unfortunate, but probably inevitable, that subjective judgement plays a role in the choice of an equilibrium criterion; similar problems are discussed by Rallison & Acrivos.

At low field strengths the numerical results could be compared against analytic

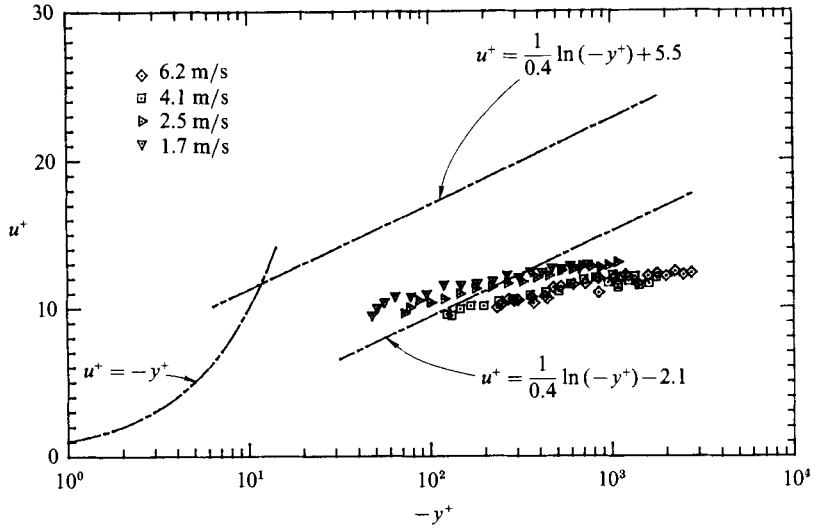

FIGURE 5. Mean horizontal velocity-defect profiles in law-of-the-wall coordinates: mechanical waves (case II).

along the wave trough (cf. Bole & Hsu 1969), thus leading to a lower mean drift velocity.

The velocity-defect profiles in wall coordinates are plotted in figure 5, together with the reference relationships cited previously for smooth- and rough-wall flows for comparison. Because the mechanically generated wave has an amplitude of about 22 mm, the closest measuring point is at least 22 mm from the mean water level. Consequently, the first data points lie at considerably greater y^+ than in Case I (figure 1).

The mean velocity profiles are logarithmic (figure 5). Although the slopes of the profiles are not 2.5 ($=1/0.4$), they are practically identical to those in the high-wind-speed wind-wave experiments. It is reasonable, then, to conclude that the significant velocity scales are u_* and $\bar{u}_S$ (as before) and that the velocity-defect distribution varies with $-\kappa y$. Of course, the value of κ is not equal to that usually taken by the von Kármán constant (0.4) because the velocity profiles have a different slope. However, κ is of the same order as 0.4. At $u_\infty = 1.7$ and 2.5 m/s, the profiles deviate from the logarithmic regions as the interface is approached (i.e. small $-y^+$). The data near this region behave as if the profiles were in a viscous sublayer, but at a higher $-y^+$ than the expected, $-y^+ \sim 11$. This results from the water motion following the surface motion of the mechanical wave (see Cheung 1984). The defining lengthscale for the mean flow boundary layer remains δ which defines the zone over which there is a substantial mean velocity gradient. The growth of the boundary layer is related, of course, to another lengthscale – the fetch – but that relationship is not explored here.

The gradient of mean vertical velocity with depth is very much smaller than the gradient of the mean horizontal velocity. The mean vertical velocities (not shown) are within ± 2 mm/s about zero for the two low-wind-speed experiments, and ± 6 mm/s at higher wind speeds.

As noted above, the data sets $f' = f_R + f_T$ were constructed by phase averaging, but now f' represents *both* the wind-generated ripple-induced (f_R) and the turbulent motions (f_T). As an example, the u'_{rms} profiles are presented in figure 6 using the same

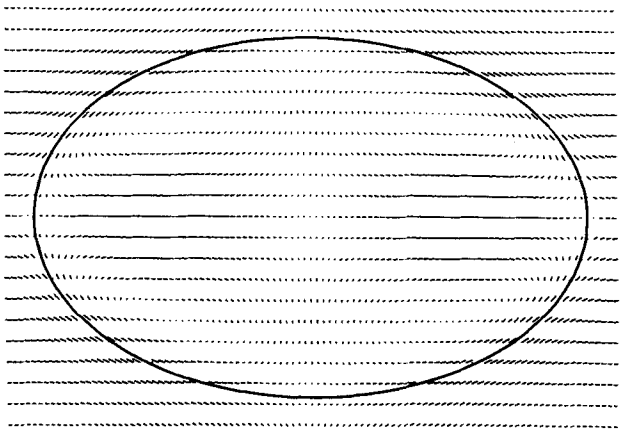

FIGURE 5. $\sigma_1/\sigma_2 = 25$, $\epsilon_1/\epsilon_2 = 1$. The drop shape and velocity field at equilibrium, when $E^{*2} = 0.24$. Circulation is clockwise in the upper right-hand quadrant of the drop. The lines represent velocity vectors, and overlap slightly in regions of high velocity. The origins of the vectors lie on a rectangular grid.

taking the limit $\epsilon_1 \to \infty$. Drop breakup occurs via an instability at the tip of the drop, and the shape at the moment of breakup is shown on figure 4. The critical field strength E^* at breakup is 0.454. This is in good agreement with the results of Brazier-Smith (1971) ($E^* = 0.452$) and Taylor (1964) ($E^* = 0.458$). Minimum-energy arguments predict $E^* = 0.453$. Just before breakup, the equilibrium length varies rapidly with E^*, and agreement on the predicted aspect ratio is poorer. The largest equilibrium aspect ratio obtained by our simulations was $l/b = 1.7$. Brazier-Smith obtained 1.83, minimum-energy arguments predict 1.85, and Taylor predicted 1.9.

The minimum-energy argument predicts that hysteresis should occur when $\kappa = 20.8$. On plotting the aspect ratio l/b as a function of E^{*2} (as in figure 2), our own simulations give deformation curves which vary continuously up to a critical value which lies in the range 19.6–19.7. This refines the bounds 19–20 obtained by Miksis. When $\kappa = 20$, there is a continuous variation of aspect ratio up to $E^{*2} = 0.36$, $l/b = 1.94$. If the field strength is increased to $E^{*2} = 0.38$, the aspect ratio increases to 4.8. It is then possible to move along the upper branch of the deformation curve, and to jump back to the lower branch. On returning to the lower curve, aspect ratios were generally slightly higher (e.g. at $E^{*2} = 0.25$, $l/b = 1.3$ for E^* increasing, 1.45 for E^* decreasing). This difference is presumably linked with the difficulty in defining equilibrium and choice of $u_{\max}$.

At $\kappa = 25$ however, it proved impossible to follow the jump to the upper branch of the deformation curve. Above the critical strength $E^{*2} = 0.31$ ($l/b = 2.3$) the drop would lengthen, up to $l/b = 3.9$. A pointed tip then developed and the numerical scheme broke down. Reducing the time step, or the increase in E^* above the critical value, did not modify this behaviour. Equilibrium solutions on the upper branch of the deformation curve could be obtained if the drop shape was initially sufficiently close to equilibrium. However, the jump from the upper branch of the deformation curve to the lower branch could not be followed when the field strength was reduced. Numerical problems were encountered at the tip of the drop. Long slender drops in an extensional flow will break into a series of droplets when the flow is stopped (Taylor 1934), and it is quite possible that we are predicting such a breakup when the field is reduced.

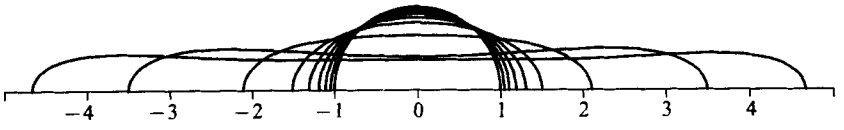

FIGURE 6. $\sigma_1/\sigma_2 = 5$, $\epsilon_1/\epsilon_2 = 1$. Equilibrium drop shapes at $E^{*2} = 0$, [0.1], 0.8.

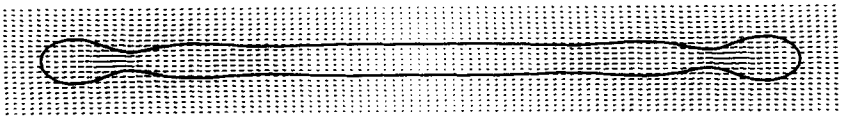

FIGURE 7. $\sigma_1/\sigma_2 = 25$, $\epsilon_1/\epsilon_2 = 1$, $E^{*2} = 0.26$. The drop is still growing slowly. Lines indicate velocity vectors, as on figure 5.

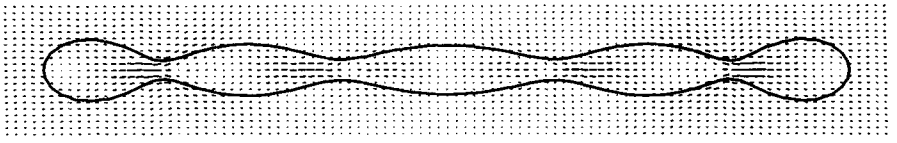

FIGURE 8. $\sigma_1/\sigma_2 = 20$, $\epsilon_1/\epsilon_2 = 1$, $E^{*2} = 0.28$. The drop is no longer extending, and is breaking into individual droplets. Lines indicate velocity vectors, as on figure 5.

Thus we have not been able to follow the hysteresis observed by Bacri & Salin. They estimate a ratio of permeabilities μ_1/μ_2 of order 40 in their experiments. As the field increased, the volume of the drop decreased in their experiments by a factor which might sometimes be as high as 2. The major difference between the experiments and the simulations is the ratio of the viscosities. In the experiments the concentrated phase forming the drop was considerably more viscous than the surrounding fluid. A concentrated ferrofluid might typically have a viscosity twenty times that of water, while $\mu_1^* = \mu_2^*$ in the simulations.

We now turn to the problem in which the conductivities of the fluids are non-zero. Even at equilibrium the fluid will be in motion, and we scale time by choosing $\mu^* = 1$. This motion is illustrated in figure 5, which shows the drop shape and velocity field at equilibrium for the case $\sigma_1/\sigma_2 = 25$, $\epsilon_1/\epsilon_2 = 1$, $E^{*2} = 0.24$. We must consider the behaviour of the drop as a function of both σ_1/σ_2 and of ϵ_1/ϵ_2, and the results presented below are summarized on figure 10.

We first fix $\epsilon_1/\epsilon_2 = 1$, constant, and consider various values of σ_1/σ_2. Figure 6 shows equilibrium shapes when $\sigma_1/\sigma_2 = 5$, $\epsilon_1/\epsilon_2 = 1$. The drop has not burst and deformation is smooth. When the field in figure 5 ($\sigma_1/\sigma_2 = 25$, $\epsilon_1/\epsilon_2 = 1$) is increased from $E^{*2} = 0.24$ to $E^{*2} = 0.26$, the drop initially lengthens rapidly, and then attains the form shown in figure 7, which is not in equilibrium, although the velocity at the ends is small. The drop is dividing into two blobs separated by a thin thread, and circulation caused by the electric field creates asymmetry in the flow at the necks where breakup will occur. This is precisely the form of breakup observed in figure 9 of Torza *et al.* This breakup is shown even more clearly in figure 8, where $\sigma_1/\sigma_2 = 20$, $\epsilon_1/\epsilon_2 = 1$.

If the drop conductivity becomes very large, the electric field within the drop becomes small. In particular, the tangential field, and thus the tangential stress, becomes small. Thus drop deformation is controlled by the normal stresses, and the

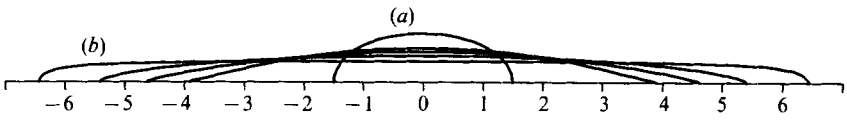

FIGURE 9. $\sigma_1/\sigma_2 = 25$, $\epsilon_1/\epsilon_2 = 14$. Equilibrium shapes, (*a*) $E^{*2} = 0.28$, (*b*) 0.3. Additional, intermediate shapes show drop deformation when E^{*2} is increased from 0.28 to 0.3. The drop tip nearly becomes conical.

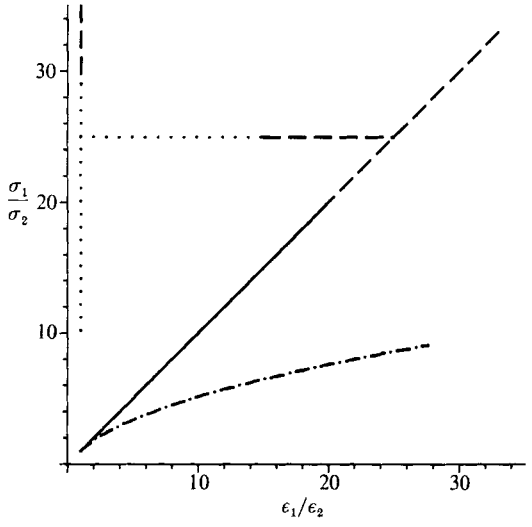

FIGURE 10. The ultimate behaviour of the drop, as a function of ϵ_1/ϵ_2 and σ_1/σ_2. ——, smooth deformation; – – –, formation of a conical tip; ·····, conical tip prevented by recirculating eddies; —·—, no deformation.

ends of the drop become pointed. The limiting ratio of conductivities that divides the two mechanisms lies between 28–29 when $\epsilon_1 = \epsilon_2$.

When $\sigma_1/\sigma_2 = \epsilon_1/\epsilon_2$ there is no build-up of charge at the interface, and the deformation is the same as for perfect dielectric fluids. If we hold σ_1/σ_2 constant, and reduce ϵ_1/ϵ_2, the mechanism of breakup varies from one determined by permittivity to one controlled by conductivity. Thus, when $\sigma_1/\sigma_2 = 25$, $\epsilon_1/\epsilon_2 = 25$, the drop becomes pointed, as discussed above for the case $\epsilon_1/\epsilon_2 = 25$, $\sigma_i = 0$. When ϵ_1/ϵ_2 is reduced to 15, the drop tip still becomes conical and the numerical simulation breaks down. In figure 9, $\sigma_1/\sigma_2 = 25$, $\epsilon_1/\epsilon_2 = 14$. The drop tip becomes almost conical, but the tangential stresses caused by conductivity are sufficient to avoid a perfect cone followed by breakup. Thus the drop survives. Finally, reverting to figure 7, we have $\epsilon_1/\epsilon_2 = 1$, with σ_1/σ_2 still equal to 25. Deformation is smooth.

In all the examples considered above, the drop deforms into a prolate spheroid. In the case $\sigma_1/\sigma_2 = 0.2$, $\epsilon_1/\epsilon_2 = 1$, circulation occurs in the reverse direction to that in figures 5–9. The deformation due to fluid circulation is opposite to, and stronger than, that due to the normal electric stresses, and the drop shape therefore approximates to an *oblate* spheriod. Such oblate spheroids have been observed to break by folding and twisting (Allan & Mason 1962). The present numerical scheme is therefore not well suited to the oblate case, since we have assumed that the drop is symmetric and that its shape $R(z)$ is a single-valued function of z. Numerical

difficulties were encountered at a field strength $E^{*2} = 0.32$ (aspect ratio 0.85), and the study of the oblate case was not pursued further.

The above results are summarized on figure 10, which shows the ultimate behaviour of the drop as a function of its position on the $(\epsilon_1/\epsilon_2, \sigma_1/\sigma_2)$-plane. We have seen that deformation into both prolate and oblate shapes is possible. Taylor (1966) showed that for suitable ratios of the conductivities, permittivities and viscosities, the drop remains spherical. When the viscosities of the two fluids are equal, this occurs when

$$7\frac{\epsilon_1}{\epsilon_2} = 2\left(\frac{\sigma_1}{\sigma_2}\right)^2 + 3\frac{\sigma_1}{\sigma_2} + 2,$$

and this curve is also shown on figure 10.

Torza *et al.* divide breakup into two classes. In the purely electric class the electric stresses dominate; fluid motion is important in the case of electrohydrodynamic breakup. My results support this view, though my classification of any individual experimental result would not necessarily be the same as theirs. Thus in figure 9 of Torza *et al.* the drop breaks into two blobs joined by a thread, while in their figure 11 tip-streaming occurred. I would clasify these as electrohydrodynamic and electric breakup, respectively, while Torza *et al.* adopted the opposite classification.

I am grateful to Dr E. J. Hinch for supplying details of the numerical scheme of Duffy & Hinch, and I thank also Dr J.-C. Bacri & Dr D. Salin for stimulating discussions.

REFERENCES

ABRAMOWITZ, M. & STEGUN, I. A. 1972 *Handbook of Mathematical Functions*. Dover.

ALLAN, R. S. & MASON, S. G. 1962 Particle behaviour in shear and electric fields: I Deformation and burst of fluid drops. *Proc. R. Soc. Lond.* A **267**, 45.

ARKHIPENKO, V. I., BARKOV, Y. D. & BASHTOVOI, V. G. 1978 Shape of a drop of magnetized fluid in a homogeneous magnetic field. *Magnetohydrodyn.* **14**, 373.

BACRI, J. C. & SALIN, D. 1982 Instability of ferrofluid magnetic drops under magnetic field. *J. Phys. Lett.* **43**, L649.

BACRI, J. C. & SALIN, D. 1983 Dynamics of the shape transition of a magnetic ferrofluid drop. *J. Phys. Lett.* **44**, L415.

BACRI, J. C., SALIN, D. & MASSART, R. 1982 Shape of the deformation of ferrofluid droplets in a magnetic field. *J. Phys. Lett.* **43**, L179.

BORZABADI, E. & BAILEY, A. G. 1978 The profiles of axially symmetric electrified pendent drops. *J. Electrostatics* **5**, 369.

BRAZIER-SMITH, P. R. 1971 Stability and shape of isolated and pairs of water drops in an electric field. *Phys. Fluids* **14**, 1.

BRAZIER-SMITH, P. R., JENNINGS, S. G. & LATHAM, J. 1971 An investigation of the behaviour of drops and drop-pairs subjected to strong electrical forces. *Proc. R. Soc. Lond.* A **325**, 363.

COWLEY, M. D. & ROSENSWEIG, R. E. 1967 The interfacial stability of a ferromagnetic fluid. *J. Fluid Mech.* **30**, 671.

DROZDOVA, V. I., SKROBOTOVA, T. V. & CHEKANOV, V. V. 1979 Experimental study of the hydrostatics characterizing the interphase boundary in a ferrofluid. *Magnetohydrodyn.* **15**, 12.

GARTON, C. G. & KRASUCKI, Z. 1964 Bubble in insulating liquids: stability in an electric field. *Proc. R. Soc. Lond.* A **280**, 211.

KOZHENKOV, V. I. & FUKS, N. A. 1976 Electrohydrodynamic atomisation of liquids. *Russ. Chem. Rev.* **45**, 1179

LADYZENSKAYA, O. A. 1969 *The Mathematical theory of Viscous Incompressible Flow*, 2nd edn. Gordon & Breach.

MACKAY, W. A. 1931 Some investigations on the deformation and breaking of water drops in strong electric fields. *Proc. R. Soc. Lond.* **133**, 565.

MELCHER, J. R. 1963 *Field-coupled Surface Waves.* MIT Press.

MELCHER, J. R. 1981 *Continuum Electromechanics.* MIT Press.

MELCHER, J. R. & TAYLOR, G. I. 1969 Electrohydrodynamics: a review of the role of interfacial shear stress. *Ann. Rev. Fluid Mech.* **1**, 111.

MIKSIS, M. J. 1981 Shape of a drop in an electric field. *Phys. Fluids* **24**, 1967.

O'KONSKI, C. T. & THACHER, H. C. 1953 The distortion of aerosol droplets by an electric field. *J. Phys. Chem.* **57**, 955.

RALLISON, J. M. 1981 A numerical study of the deformation and burst of a viscous drop in general shear flows. *J. Fluid Mech.* **109**, 465.

RALLISON, J. M. & ACRIVOS, A. 1978 A numerical study of the deformation and burst of a viscous drop in an extensional flow. *J. Fluid Mech.* **89**, 191.

STRATTON, J. A. 1958 *Electromagnetic Theory.* McGraw-Hill.

TAYLOR, G. I. 1934 The formation of emulsions in definable fields of flow. *Proc. R. Soc. Lond.* A **146**, 501.

TAYLOR, G. I. 1964 Disintegration of water drops in an electric field. *Proc. R. Soc. Lond.* A **280**, 383.

TAYLOR, G. I. 1966 The circulation produced in a drop by an electric field. *Proc. R. Soc. Lond.* A **291**, 159.

TAYLOR, G. I. & MCEWAN, A. D. 1965 The stability of a horizontal fluid interface in a vertical electric field. *J. Fluid Mech.* **22**, 1.

TORZA, S., COX, R. G. & MASON, S. G. 1971 Electrohydrodynamic deformation and bursts of liquid drops. *Phil. Trans. R. Soc. Lond.* A **269**, 295.

VONNEGUT, B. & NEUBAUER, R. L. 1952 Production of monodisperse liquid particles by electrical atomization. *J. Colloid. Sci.* **7**, 616.

WILSON, C. T. R. & TAYLOR, G. I. 1925 The bursting of soap bubbles in a uniform electric field. *Proc. Camb. Phil. Soc.* **22**, 728

YOUNGREN, G. K. & ACRIVOS, A. 1975 Stokes flow past a particle of arbitrary shape: a numerical method of solution. *J. Fluid Mech.* **69**, 377, and Corrigenda, *J. Fluid Mech.* **69**, (1975) 813.